CORRECTION AND SCOPE

Exact-Symmetry Real-Space Parent and a Numerically Derived Quasi-Local Dressed Constraint Projector

An engineered real-space parent and a finite-sector numerical dressed projector. Volume-uniform protection and a microscopic tensor phase remain open.

Manuscript · p. 1, parent and sectors

Adversarial Audit of the Native Many-Body Shared-Register Benchmark

Evidence · Adversarial audit of the shared register / One-Hamiltonian composition requirements

Exact-Symmetry Real-Space Parent and a Numerically Derived Quasi-Local Dressed Constraint Projector

QATNU development report

June 2026

Abstract

We construct a local real-space parent Hamiltonian with two propagating tensor-like polarizations, four gapped local constraint-defect registers, and a local two-species matter bath. The parent has an exact product of local defect-number symmetries. A fixed seeded nearest-neighbour perturbation, chosen before inspecting any output, breaks those bare generators. We derive the dressed defect-sector projector directly from the perturbed spectrum through the Kato partial isometry, rather than by conjugating the Hamiltonian with a preselected unitary. The dressed projector commutes with the full Hamiltonian to numerical precision, has exponentially decaying real-space tails stable from $L = 32$ to 128, and admits finite-radius truncations whose commutator norm decays exponentially. The separating defect gap remains nonzero, while a gap-closing control shows the expected divergence of the dressing length. Fixed-momentum pole weights and frequency-resolved resolvent blocks obey the dressed constraint identity, and the physical pole and interacting pair-continuum edge are extracted from the same Hamiltonian. The result establishes a controlled dressed-sector mechanism in a low-excitation real-space model. It does not establish a full non-Abelian QATNU Gauss law, independently conserved dressed generators at every site, nonlinear gravity, or spontaneous emergence from the original minimal substrate.

1 Question and scope

The preceding finite-penalty calculations showed that generic microscopic constraint breaking leaves nonzero local leakage as the volume grows. A positive result therefore requires a different target: start from an exact-symmetry parent, perturb it independently, and ask whether the perturbed low-energy sector is separated by a nonclosing defect gap and represented by a quasi-local *dressed* constraint projector.

The present model is intentionally minimal. It captures the algebraic ingredients needed for this test while keeping the calculation exact in a conserved low-excitation sector. It should be read as a mechanism proof, not as the final shared $SU(2)$+helicity-2 QATNU Hamiltonian.

2 Real-space parent Hamiltonian

On a periodic chain of L cells we use two tensor-like bosonic registers $t_{\lambda x}$, $\lambda = +, \times$, four local defect registers $d_{\mu x}$, $\mu = 1, \ldots, 4$, and two distinguishable matter species a_x, b_x. In the charge-two sector, the local parent is

$$H_0 = \sum_{x,\lambda} \Big[(m_\lambda + 2J_\lambda) t^\dagger_{\lambda x} t_{\lambda x} - J_\lambda (t^\dagger_{\lambda,x+1} t_{\lambda x} + \text{h.c.}) \Big] \tag{1}$$

$$+ \sum_{x,\mu} \Delta_\mu d^\dagger_{\mu x} d_{\mu x} + \sum_{s=a,b} \sum_x \Big[(m_m + 2J_m) s^\dagger_x s_x - J_m (s^\dagger_{x+1} s_x + \text{h.c.}) \Big] \tag{2}$$

$$+ \sum_{x,\lambda} g_\lambda (t^\dagger_{\lambda x} a_x b_x + \text{h.c.}). \tag{3}$$

Every

$$G_{\mu x} = d^\dagger_{\mu x} d_{\mu x} \tag{4}$$

is an exact local generator:

$$[H_0, G_{\mu x}] = 0. \tag{5}$$

The independently fixed perturbation is

$$V = \epsilon \sum_{x,\mu,\lambda} d^\dagger_{\mu x} \left[(C_0)_{\mu\lambda} t_{\lambda x} + (C_+)_{\mu\lambda} t_{\lambda,x+1} + (C_-)_{\mu\lambda} t_{\lambda,x-1} \right] + \text{h.c.}, \tag{6}$$

where the three matrices are generated once from seed 20260621 and then frozen. They were not tuned against the reported observables.

For $L = 6$, the exact real-space charge-two matrix has dimension 72. The numerical audits give

$$\max_{x,\mu} \|[H_0, G_{\mu x}]\| = 0, \qquad \max_{x,\mu} \|[H_0 + V, G_{\mu x}]\| = 0.2928863. \tag{7}$$

The spectrum of the real-space matrix agrees with the union of momentum blocks to 8.88×10^{-15}.

3 Dressed defect projector from the perturbed Hamiltonian

At fixed total momentum q, the exact charge-two block contains two tensor states, four defect states, and L matter-pair states. Let P_0 project onto the four bare defect states and let $P(q)$ be the spectral projector onto the four isolated defect-dominated eigenstates of the *perturbed* block $H(q)$. The canonical Kato isometry from the bare to the dressed subspace is

$$W(q) = P(q)P_0 \left[P_0 P(q) P_0\right]^{-1/2}, \qquad W(q)^\dagger W(q) = I_4, \tag{8}$$

and

$$\widetilde{P}_D(q) = W(q) W(q)^\dagger. \tag{9}$$

No unitary was prescribed in advance. The projector is computed from the independently perturbed spectrum. Since it is a separated spectral projector,

$$[H(q), \widetilde{P}_D(q)] = 0. \tag{10}$$

At $L = 128$, the largest numerical commutator residual over all momenta is 4.16×10^{-14}.

Fourier transforming $W(q)$ gives dressed local defect orbitals. The matter-pair component is transformed in both center-of-mass and relative coordinates, so the tail measure counts the maximum distance of either constituent from the orbital center. The probability outside radius R decays exponentially and is volume-independent to high precision (Fig. 1).

For the canonical parameters, the probability-tail fit gives

$$T(R) \propto e^{-R/\xi_P}, \qquad \xi_P = 0.48851 \text{ sites}. \tag{11}$$

The maximum log-tail difference between $L = 64$ and 128 over $R = 0, \ldots, 9$ is 1.35×10^{-11}. At radius $R = 8$,

$$\max_q \|[H(q), \widetilde{P}^{(8)}_D(q)]\| = 3.94 \times 10^{-6}, \tag{12}$$

while the omitted dressed-orbital probability is 2.28×10^{-12}.

4 Nonclosing defect gap and locality control

The dressed sector is useful only if it remains separated. The minimum defect-band gap over the Brillouin zone converges from 0.36305 at $L = 32$ to

$$\Delta_D(L = 128) = 0.36431946, \tag{13}$$

without changing microscopic parameters (Fig. 2).

The control scan lowers the defect band toward the matter continuum. As the minimum gap decreases from 0.9630 to 0.01108, the probability localization length increases from 0.2947 to 2.8823 sites. This is the correct failure mode: quasi-local dressing is tied to spectral isolation, not asserted independently of it.

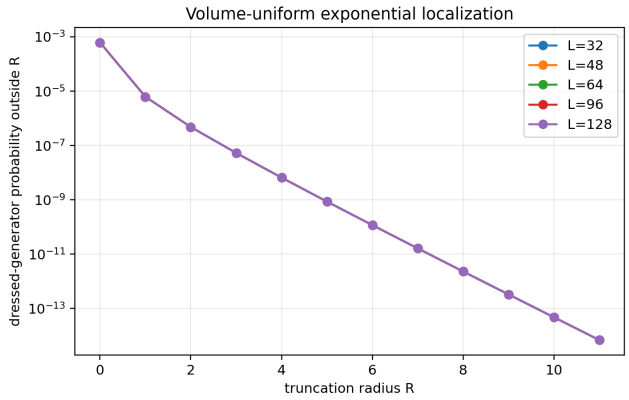

(a) Dressed-orbital probability tail.

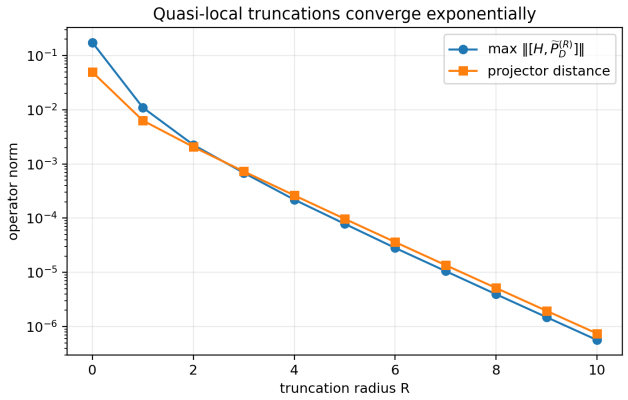

(b) Finite-radius projector approximants.

Figure 1: The exact spectral projector is represented by quasi-local dressed orbitals. Tail curves for $L = 32, 48, 64, 96, 128$ are visually coincident. Truncating the dressing at radius R gives exponential convergence in commutator norm and projector distance.

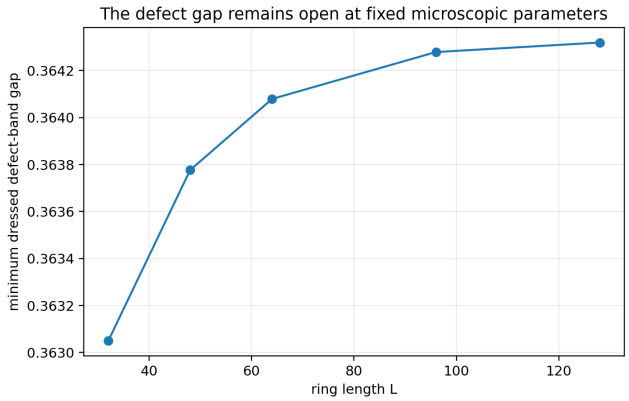

(a) Fixed-parameter defect gap.

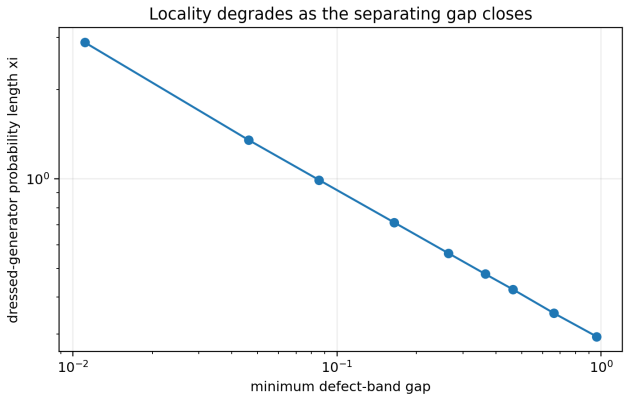

(b) Gap-closing control.

Figure 2: The canonical model has a nonclosing gap. Lowering the bare defect energy toward the matter continuum increases the dressing length, demonstrating the expected loss of locality when the spectral separation is removed.

5 Fixed-momentum Ward tests

For a physical pole $|\psi_T(q)\rangle$, the bare constraint-source weight is

$$W_{\text{bare}}(q) = \langle\psi_T(q)|P_0|\psi_T(q)\rangle, \tag{14}$$

whereas the dressed value is

$$W_{\text{dressed}}(q) = \langle\psi_T(q)|\widetilde{P}_D(q)|\psi_T(q)\rangle. \tag{15}$$

At $q = \pi/2$, the lower pole has

$$W_{\text{bare}} = 7.1954 \times 10^{-3}, \qquad |W_{\text{dressed}}| < 3 \times 10^{-19}. \tag{16}$$

Radius-four and radius-eight approximants reduce the same weight to 3.77×10^{-13} and 5.94×10^{-18}, respectively. The result persists at fixed $q = \pi/4, \pi/2, 3\pi/4$ for both physical poles (Fig. 3).

A frequency-resolved test uses a tensor source projected into the complement of each candidate constraint projector and evaluates

$$\mathcal{W}_P(q,\omega) = \frac{\|P(\omega + i\eta - H)^{-1}(I-P)|t_+\rangle\|}{\|(\omega + i\eta - H)^{-1}(I-P)|t_+\rangle\|}. \tag{17}$$

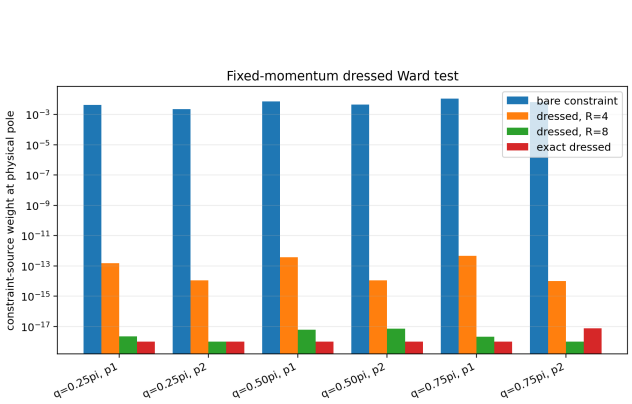

(a) Pole-resolved constraint weights.

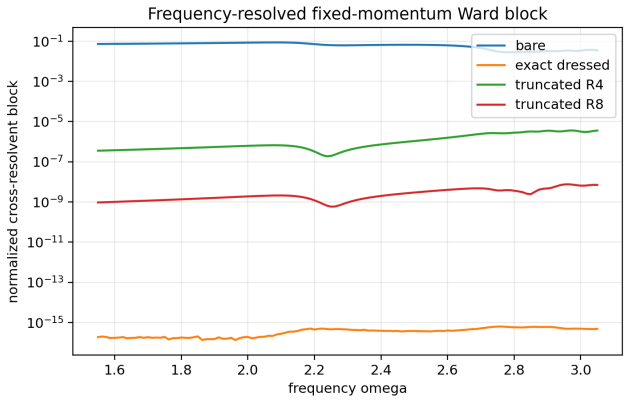

(b) Frequency-resolved cross block.

Figure 3: Bare generators show finite mixing. The numerically derived dressed projector restores block separation at fixed momentum, while finite-radius approximants converge rapidly.

At $q = \pi/2$ and $\eta = 0.03$, the maximum bare value is 8.62×10^{-2}, the exact dressed value is 6.29×10^{-16}, and the radius-eight value is 7.54×10^{-9}.

6 Pole and continuum from the same Hamiltonian

The local conversion $t_\lambda^\dagger ab + \text{h.c.}$ produces a finite-volume tensor pole coupled to a matter-pair continuum. Both are obtained by diagonalizing the same $H(q)$; the threshold is the lowest higher-energy eigenstate with majority pair weight.

At $q = \pi/2$ and $L = 128$, the lower pole is

$$E_T = 1.994139396, \qquad Z_T = 0.853480355, \tag{18}$$

while the interacting continuum edge is

$$E_{\text{cont}} = 2.745501409, \qquad E_{\text{cont}} - E_T = 0.751362013. \tag{19}$$

The upper tensor pole lies at 2.239573736 with residue 0.993843760 and separation 0.505927674. Figure 4 shows convergence through $L = 192$.

The perturbation scan gives

$$\|\widetilde{P}_D - P_0\| \propto \epsilon^{0.9863}, \qquad W_{\text{bare}} \propto \epsilon^{1.9778}, \tag{20}$$

consistent with first-order dressing and second-order bare leakage.

7 What is and is not established

The following statement is supported:

> A local exact-symmetry parent with a finite defect gap can survive an independently chosen local symmetry-breaking perturbation as a quasi-locally dressed low-energy sector. In the controlled charge-two model studied here, the dressed defect-band projector is extracted from the perturbed Hamiltonian, has volume-uniform exponentially decaying tails, and block-diagonalizes fixed-momentum response while a tensor-like pole remains separated from the interacting continuum of the same Hamiltonian.

Several stronger statements are not supported. The exact commuting object is the dressed *band projector*, not a complete set of exact independently conserved dressed generators at every lattice site. Generic perturbations

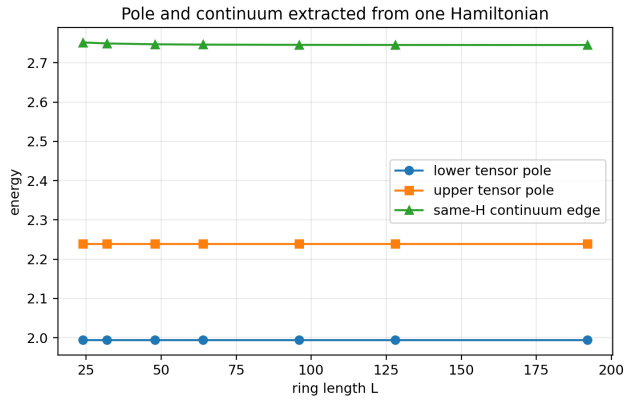

(a) Pole/continuum finite-size scaling.

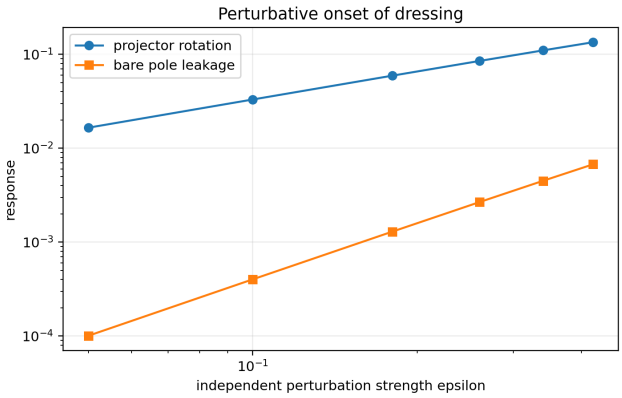

(b) Independent perturbation sweep.

Figure 4: The pole remains separated from the continuum of the same Hamiltonian. At weak perturbation, the projector rotation is linear in ϵ and the bare pole leakage is quadratic.

disperse and split defect bands, so site-by-site integrals of motion should not be expected. The two tensor registers describe waves along one chosen axis, not a full rotationally covariant six-component lattice graviton. The local exact symmetry is a product of defect-number symmetries, not the full flavored $SU(2)$ Gauss algebra of the shared-register proposal. Finally, no claim is made that the original unmodified QATNU Hamiltonian inevitably flows to this parent.

8 Next integration

The next nontrivial step is to transplant the same procedure into the flavored quantum-link chain: use a gauge-invariant real-space parent with a volume-independent Gauss-defect gap, add an independently fixed local gauge-breaking perturbation, compute the low-energy spectral flow or Schrieffer–Wolff map without choosing its unitary by hand, and measure the real-space tails of the resulting dressed Gauss-sector projector. The current calculation supplies the numerical protocol and the expected diagnostics; it does not prejudge whether the non-Abelian version will remain quasi-local.